Journal of Membrane Science 563 (2018) 785–793

Contents lists available at ScienceDirect

Journal of Membrane Science

journal homepage: www.elsevier.com/locate/memsci

Water and salt dynamics in multilayer graphene oxide (GO) membrane: Role of lateral sheet dimensions

Abhijit Gogoi[a], Tukhar Jyoti Konch[b], Kalyan Raidongia[b], K. Anki Reddy[c,*]

[a] Department of Mechanical Engineering, Indian Institute of Technology, Guwahati 781039, Assam, India
[b] Department of Chemistry, Indian Institute of Technology, Guwahati 781039, Assam, India
[c] Department of Chemical Engineering, Indian Institute of Technology, Guwahati 781039, Assam, India

ARTICLE INFO

Keywords:
Multilayer GO membrane
Water permeability
Salt rejection
Molecular dynamics simulation
Pore offset distance

ABSTRACT

Dependence of salt rejection efficiency and water permeability of layered graphene oxide (GO) membranes on the lateral dimension of constituting sheets are studied through equilibrium molecular dynamic (MD) simulation and experiments. This study suggests that with increasing sheets dimension permeability of the GO membranes decreases but its selectivity increases. The velocity and permeation time of the water molecules while permeating through the membrane are influenced to a greater extent by the pore offset distance (**W**) of the membranes. More over the larger pore offset distance increases the path length that the water molecules and ions have to traverse for permeating through the layered GO membranes. Based on the simple technique discussed in this work, one can construct GO membranes of required water permeability and salt rejection without the application of any foreign nanomaterials with the GO membrane, which retains the inherent selectivity of the GO membranes. This work also provides the effect of internal structure of GO membrane on the atomistic level details of the solvation shell of ions while they are permeating through the membrane.

1. Introduction

The growing demand of fresh water with the rapid growth of human civilization urges the researchers to search for efficient and cost effective water desalination/purification techniques. On this important note, Graphene oxide (GO), a unique blend of hydrophilic and hydrophobic nano-regime confined at strictly two-dimensional sheet morphology [1] has emerged as one of the most extensively studied materials in the last decade [2–4]. Removal of solvent molecules from GO dispersions yields a layered structure and the interlayer spacing between the GO layers serves as the nano-channel for water permeation [5–11]. Due to its extremely large lateral dimensions, GO sheets readily self-assemble into freestanding lamellar membranes, where the interlayer spacing between the sheets serves as an interconnected network of ionic and/or molecular channels [12,13]. Experimentally the interlayer distance between stacked GO sheets was found to be ranged from 6 to 11 Å [14,15]. Wei et al. [4] found the interlayer separation between the GO sheets ranges from 7.5 Å to 12.4 Å in their molecular dynamics simulations. The water diffusivity increases with an increase in interlayer distance between the successive GO layers [16]. This interlayer distance can be suitably altered [17–19] to get the desired water permeation and salt rejection.

The highly selective nature of the GO membrane is mainly attributed to its unique structure [20]. The selectivity of the GO membrane is achieved by the size exclusion from the interlayer spacing, electrostatic interactions between the ions and the negatively charged GO nanosheets, cation-π interaction, metal coordination of the GO nano-sheet and among others. Based on the selectivity pertained to the size exclusion from the interlayer spacing in the layered GO membrane, molecules and ions can be separated according to their hydrated radius and ions with a hydrated radius > 4.5 Å are not able to permeate through the GO membranes [21].

Recently a scalable production method for GO membrane has been addressed [22] that maintain large diameter graphene oxide flakes (> 100 μm) with high oxygen-to- carbon ratios (> 40%). Similarly, a synthetic tree that incorporates a GO membrane has recently been designed [23] which allows water to be moved passively using the same mechanisms as terrestrial plants. GO can also be combined with other membrane materials to obtain homogeneous membrane matrix [24,25] for enhancement of membrane functionality. GO membrane possess several interesting advantages over existing commercially available membrane [26,27] e.g., lower membrane fabrication cost, simple and scalable synthesis procedure, high water permeability, exceptional selectivity among others. Another advantage of GO membrane is that in

* Corresponding author.
E-mail addresses: k.raidongia@iitg.ac.in (K. Raidongia), anki.reddy@iitg.ac.in (K. Anki Reddy).

https://doi.org/10.1016/j.memsci.2018.06.031
Received 13 February 2018; Received in revised form 4 June 2018; Accepted 16 June 2018
Available online 19 June 2018
0376-7388/

the presence of multivalent metal cations (which may present in seawater/wastewater) the cross linking of the GO layers takes place [28] which ensures structural stability in aqueous solutions. Previous experimental observations also support the high water permeability and highly selective nature of GO membranes [29–32]. The fast water permeation through the nano-channels of a GO membrane is mainly attributed to the frictionless interaction between the atomically smooth, hydrophobic carbon wall and the well-ordered hydrogen bonds of the water molecules that gives rise to capillary force which is strong enough to overcome the gravitational force to form a thin water film on the GO deposited layers [33].

The sub-nanometer size of the channels and high charge density of sheets confer excellent ionic and molecular selectivity on GO membrane. Therefore, in the recent time, it has received tremendous attention as a potential nano-filtration membrane. However, for practical applications, membranes with high water permeability is as important as ionic/molecular selectivity. Even though the hydrophobic graphitic regions of GO support the frictionless flow of water, the overall permeability through the membrane is far less than desired. Therefore, efforts have been made to improve the permeability by increasing the channel height by applying spacers between the sheets [34]. Unfortunately, foreign spacers can not only diminish selectivity but also alter other relevant properties of the pristine GO membranes. Therefore, here we propose to tune permeability and selectivity of GO membrane just by choosing sheets of appropriate lateral dimensions. Any synthesized GO sample contain sheets of various shapes and sizes. From aqueous dispersions of GO, sheets of different lateral dimensions can be easily separated, primarily based on their weights through centrifugation [35]. Water permeation and salt rejection efficiency through GO membranes made from sheets of three different lateral dimensions are investigated here by employing both molecular dynamics (MD) simulations and experiments.

2. Molecular dynamics simulation methodology

In this present work 3 different configurations of GO membrane are considered. Initially four different sizes of single layer of GO sheets were constructed. The atomistic structure of a GO sheet is shown in Fig. 1. In the GO sheet both epoxy and hydroxyl groups are considered following the model proposed by Lerf and Klinowski [36]. The epoxy and hydroxyl groups are located on the basal plane on both side of the GO sheet and the carboxylic groups are located on the edges. The chemical composition of all the GO sheets are $C_{10}O_1(OH)_1(COOH)_{0.5}$. This composition of GO has been reported in many recent works on GO [37,38]. With this chemical composition four different sizes of GO sheets are constructed: $20 \times 49\,Å^2$, $30 \times 49\,Å^2$, $40 \times 49\,Å^2$ and $50 \times 49\,Å^2$. These single layer of 4 GO sheets are arranged in space to obtain 3 different configurations of GO membranes with different pore offset distance (**W**) using Visual Molecular Dynamics (VMD) package [39] as shown in Fig. 2. These 3 configurations are abbreviated as: configuration-1, configuration-2 and configuration-3 in the subsequent discussion.

In all the 3 types of membrane configurations the interlayer distance (**H**) and the dimensions of the pore (**D**) for water passage in a single layer are same which are 10 Å [13,14] and $7 \times 49\,Å^2$ respectively. However, the interlayer spacing between the GO nano-sheets varies from 4 Å to 7 Å. In configuration-1 the pore offset distance (**W**) between two successive layers is 25 Å (Fig. 2a), whereas for the case of configuration-2 this distance is 8 Å (Fig. 2b). In configuration-3 the center of pores between the two successive layers of GO sheets are perfectly aligned i.e. **W** = 0 (Fig. 2c). From an experimental point of view configuration-1 refers to the GO membrane composed of sheets of large lateral dimensions; configuration-2 resembles GO membrane composed of sheets of medium lateral dimensions and configuration-3 resembles GO membrane composed of sheets of very small lateral dimensions. Along with these 3 GO membrane configurations 2 additional

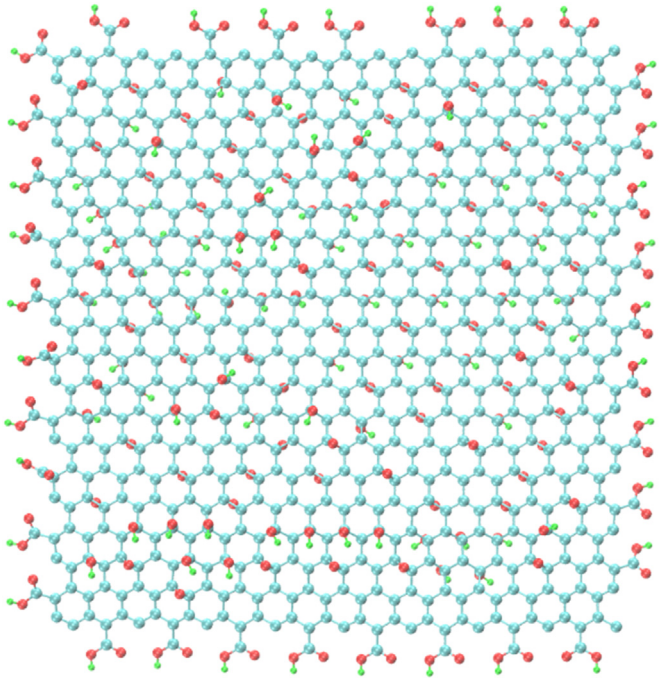

Fig. 1. Structure of GO sheet used in simulation study. Here, red color is for oxygen atoms, green color is for hydrogen atoms and cyan color is for carbon atoms (For interpretation of the references to color in this figure legend, the reader is referred to the web version of this article.).

configurations (**W** = 4 Å and **W** = 16 Å) are also considered for determining the variation of water permeability through the layered GO membranes with **W**. After the three GO membrane configurations are created they are solvated in an equilibrated water box of size $77 \times 49 \times 210\,Å^3$ for the case of simulations with pure water. For the case of simulations with NaCl solution the GO membranes are solvated in an equilibrated NaCl solution box of size $77 \times 49 \times 215\,Å^3$. The water and ion molecules which are within 2 Å from the GO sheets are removed. In all the three 3 configurations the number of water molecules are 21,300 and the number of NaCl molecules are 238 for the case of simulations with NaCl solution. Fig. 2d and Fig. 2e shows the schematic of the simulated system with pure water and NaCl solution respectively.

All the molecular dynamics simulations were performed using NAMD 2.11 [40]. The optimized potentials for liquid simulations-all atom (OPLS-AA) [41] force field is used for the simulations. Water molecules are modeled using TIP3P [42] whose bond lengths are held constant using the SETTLE algorithm [43]. The van der Waals interactions are computed through Lennard-Jones potential and were truncated and shifted at a cut-off distance r_c = 10 Å. Long range electrostatic interactions were calculated using the particle mesh Ewald method (PME) [44]. The velocity Verlet integration method is used to advance the positions and velocities of the atoms in time with a time step of 1 fs.

In OPLS-AA force field the intramolecular bonded interactions are given by the following set of potentials

$$V_b(r_{ij}) = k_{ij}^b(r_{ij} - b_0)^2 \tag{1}$$

$$V_a(\theta_{ijk}) = k_{ijk}^{\theta}(\theta_{ijk} - \theta_{ijk}^0)^2 \tag{2}$$

$$\begin{aligned} V_d(\phi_{ijkl}) &= \frac{V_1}{2}[1 + \cos(\phi + f_1)] \\ &+ \frac{V_2}{2}[1 - \cos(2\phi + f_2)] \\ &+ \frac{V_3}{2}[1 + \cos(3\phi + f_3)] \end{aligned} \tag{3}$$

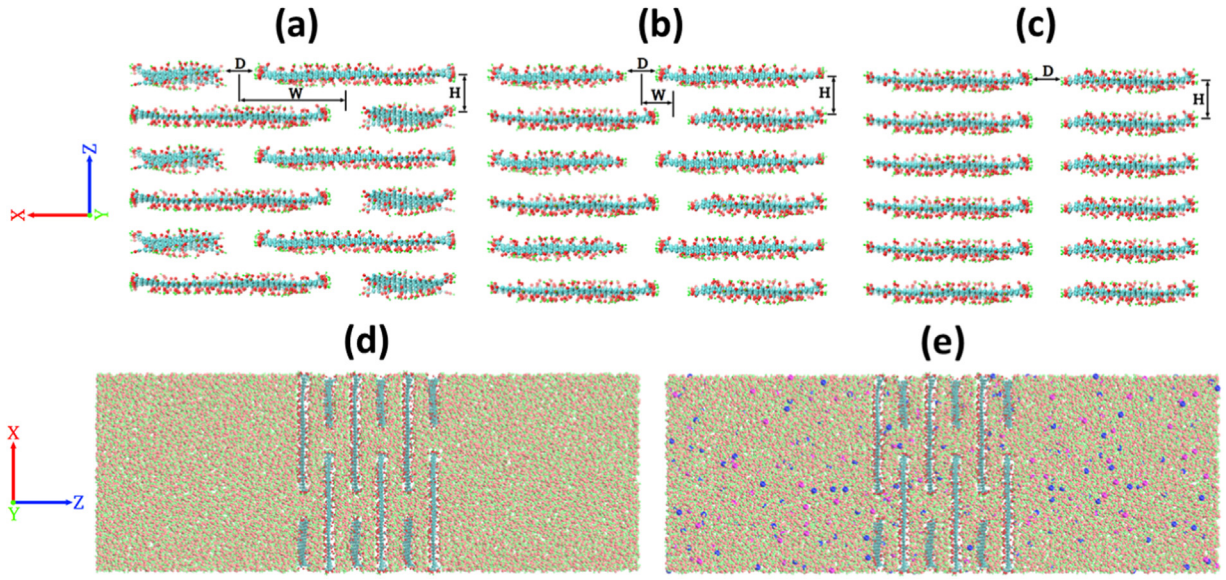

Fig. 2. The three membrane configurations; (a) configuration-1, (b) configuration-2, (c) configuration-3. (d) Representative simulation snapshot where a GO membrane (configuration-1) is solvated in pure water. (e) Representative simulation snapshot where a GO membrane (configuration-1) is solvated in NaCl solution. Red color represents oxygen atoms, green color is for hydrogen atoms, cyan color is for carbon atoms, blue color is for chloride ions and magenta color represents sodium ions (For interpretation of the references to color in this figure legend, the reader is referred to the web version of this article.).

In the above equations $V_b(r_{ij})$ represents the bond interaction between atom i and j separated by a distance r_{ij} with b_0 as the equilibrium bond distance between them and spring constant k_{ij}^b for the particular pair of bonded atoms. The angular interaction between three atoms labeled by i, j and k which are connected through two bonds with angle θ_{ijk} is given by $V_a(\theta_{ijk})$. Here θ_{ijk}^0 is the equilibrium bond angle and k_{ijk}^{θ} is the corresponding force constant. Finally, the torsional interaction due to the torsional angle ϕ_{ijkl} between the planes containing the atoms with indices i, j, k and j, k, l is given by $V_d(\phi_{ijkl})$ where V_i, $(i = 1, 2, 3...)$ is the corresponding Fourier coefficients for torsional energy functions.

In this present work two types of non-bonded interactions are considered; van der Waals interaction and Coulomb interaction. The van der Waals interaction is modeled through Lennard-Jones (LJ) potential given by

$$V_{LJ}(r_{ij}) = \frac{C_{ij}^{(12)}}{r_{ij}^{(12)}} - \frac{C_{ij}^{(6)}}{r_{ij}^{(6)}} \tag{4}$$

The parameters $C_{ij}^{(12)} = 4\varepsilon_{ij}\sigma_{ij}^{(12)}$ and $C_{ij}^{(6)} = 4\varepsilon_{ij}\sigma_{ij}^{(6)}$ depend on the pairs of atom types with the following combination rule employed for interaction between different atom types.

$$\varepsilon_{ij} = (\varepsilon_{ii}\varepsilon_{jj})^{1/2} \tag{5}$$

$$\sigma_{ij} = (\sigma_{ii}\sigma_{jj})^{1/2} \tag{6}$$

where ε_{ij} is the potential well depth and σ_{ij} is the distance where the potential equals zero.

The Coulomb interaction is given by

$$V_C(r_{ij}) = \frac{1}{4\pi\varepsilon_0}\frac{q_i q_j}{\varepsilon_r r_{ij}} \tag{7}$$

here q_i and q_j are the charges on the particle labeled by i and j, separated by a distance r_{ij}, and ε_0, ε_r are the vacuum and relative dielectric permittivity, respectively.

Before the MD simulation was started, energy minimization had been carried out. Then the system was equilibrated for 5 ns at a constant pressure of 1 atm and at a temperature of 300 K. Pressure was kept constant using modified Nosé-Hoover method in which Langevin dynamics were used to control fluctuations in the barostat. The barostat oscillation time and damping factors both were set to 0.3 ps. Temperature was controlled by using Langevin dynamics with a damping factor of 5 ps^{-1}. The equilibrated system size was $77 \times 49 \times 205$ $Å^3$ for pure water-GO system and $77 \times 49 \times 210$ $Å^3$ for NaCl solution-GO system. Then, the production MD simulations were performed in a *NVT* ensemble for 40 ns at 300 K. Periodic boundary conditions were applied in all three independent directions. During MD simulations the carbon atoms of the GO sheets are constrained with spring constant of 1 kcal mol^{-1} $Å^2$ to maintain the planner structure of the GO sheets. A lower vale of spring constant (1 kcal mol^{-1} $Å^2$) is considered to facilitate more movement of the functional groups and carbon atoms of the GO sheets during simulations.

3. Results and discussion

Through the equilibrium MD simulations, we computed the number of water permeation events took place during the course of 40 ns simulations through each of the GO membrane configurations. If a water molecule crosses the GO layer located on the top of the GO membrane, then a water permeation event in the $+z$ direction is counted. Similarly, if a water molecule crosses the GO layer located on the bottom of the GO membrane, then a water permeation event in the -*z* direction is counted. Similar is the case for ion permeations. For the simulation with NaCl solution and GO membrane system, the total number of water permeation events (***Np***) for membrane of configuration-1, in $+z$ direction is found to be 79 and in the -*z* direction it is 82. For configuration-2, ***Np*** in the $+z$ is 678 and in the -*z* direction it is 644. Similarly, for configuration-3, ***Np*** in the $+z$ and -*z* directions are 1287 and 1188 respectively. Fig. 3 depicts the number of water molecules permeated through the layered GO membrane as a function of **W** and it is observed that the reduction in the number of permeated water molecules through the membrane with increase in **W** is seemed to be parabolic in nature.

For pure water and GO membrane system ***Np*** in the $+z$ direction is 101 and ***Np*** in the -*z* direction is 90 for configuration-1. For configuration-2, ***Np*** in the $+z$ direction is 768 and ***Np*** in the -*z* direction is 700. Similarly, for configuration-3, ***Np*** in the $+z$ direction is 1387 and ***Np*** in the -*z* direction is 1423. During the simulation no ion permeation event is encountered for the configuration-1. For configuration-2, 2 Na^+ ions are permeated in the $+z$ direction and in the -*z* direction, 1 Na^+ ion and 1 Cl^- ion are permeated. No Cl^- ion has permeated in the

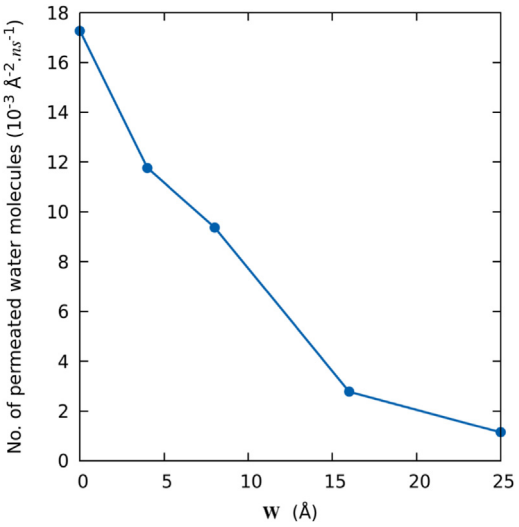

Fig. 3. Number of water molecules permeated across the layered GO membrane as a function of pore offset distance (**W**).

$+z$ direction for configuration-2. Finally, for configuration-3, 4 Na^+ ions and 4 Cl^- ions are permeated in the $+z$ direction. In the $-z$ direction, 2 Na^+ ions and 3 Cl^- ions are permeated for configuration-3. In all the three configurations of the GO membrane the water permeation events in the $+z$ direction is almost equal to the water permeation events in the $-z$ direction. This is because we are performing equilibrium MD simulation, i.e., there is no net driving potential for the water molecules across the GO membrane. However, these results clearly suggest that with the increase in pore offset distance (**W**) the water permeability of the GO membrane decreases and the salt rejection increases.

Fig. 4 shows the trajectory of the water molecules through the GO membrane. For each of the 3 GO membrane configurations, 5 individual water molecules are considered and the trajectory of each of these water molecules are shown (Fig. 4) with different colors. It is evident that water molecules have to cover more distance in configuration-1 (Fig. 4a) before they permeated through the GO membrane, followed by configuration-2 (Fig. 4b) and configuration-3 (Fig. 4c).

Fig. 5 and Fig. 6 show the trajectory of the Na^+ ion and Cl^- ion through the layered GO membrane for configuration-2. As the ions permeated through the layered GO membrane at the locations of the pores (positions 2 and 4 for both Na^+ and Cl^- ions for configuration-2 as shown in Fig. 5 and Fig. 6 respectively) the number of water molecules in the hydration shell of the ions reduces as the ions try to cross the pores between the GO layers. This could be due to the presence of more electronegative carboxylic functional groups located at the edges of the GO nano-sheets which replaces the water molecules in the hydration shell of the ions as they pass by the edges of the GO nano-sheets. In Fig. 5 if we compare position 2 and 4 with position 5 it is evident that the carboxylic functional group has more dominant effect on the hydration shell of the ions as compared to the epoxy and hydroxyl functional group located on the basal plane of the GO nano-sheets. Similarly, Fig. 7 and Fig. 8 respectively show the trajectory of the Na^+ ion and Cl^- ion inside the layered GO membrane for configuration-3. As in the case of configuration-2 here also the number of water molecules in the hydration shell of the ions reduces near the pore (positions 4, 5 for Na^+ ion in Fig. 7 and positions 2 and 5 for Cl^- ion in Fig. 8).

In Fig. 9a and Fig. 9b the number of water molecules ($\boldsymbol{N_H}$) present in the hydration shell of the ions as a function of simulation time is depicted for configuration-2 for Cl^- ion and Na^+ ion respectively. As can be seen $\boldsymbol{N_H}$ reduces while the ions are permeating through the membrane (16–25 ns for Cl^- ion and 13–36 ns for Na^+ ion). Similarly, Fig. 9c and Fig. 9d shows the variation of the $\boldsymbol{N_H}$ with simulation time for configuration-3 for Cl^- and Na^+ ion respectively. Here also $\boldsymbol{N_H}$ reduces as the ions are permeating through the membrane (16–21 ns for Cl^- ion and 5–37 ns for Na^+ ion). From Fig. 9 it is evident that the Na^+ ions are trapped inside the layered GO membrane for a longer duration of time as compared to the Cl^- ions which can be attributed to the cation-π interaction between the Na^+ ions and π-electrons of the GO nano-sheets.

Fig. 10 shows the distribution of distance traversed, time taken by the water molecules and their corresponding velocity while permeating through the GO membranes for the NaCl solution and GO membrane system. Figs. 10a, 10b, 10c shows the distribution of the distance traversed by the water molecules while permeating through the GO membrane for the three different configurations. For configuration-1 the average distance traversed by the water molecules for permeation is 827.96 nm per water molecule, for configuration-2 it is 764.88 nm per water molecule and for configuration-3 this value is 754.74 nm per water molecule. We also computed the average time taken by the water molecules to permeate through the GO membrane. The average time for permeation for configuration-1 is 25.40 ns per water molecule, for configuration-2 is 19.89 ns per water molecule and for configuration-3 is 18.57 ns per water molecule. Figs. 10d, 10e, 10f shows the distribution of the time taken by the water molecules to permeate through the GO membrane for the three different configurations. The average velocity of the water molecules permeating through the GO membrane of configuration-1 is 32.03 nm/ns, configuration-2 is 36.20 nm/ns and configuration-3 is 38.93 nm/ns. Figs. 10g, 10h, 10i shows the permeation velocity distribution of the water molecules that were permeated through the layered GO membranes.

From Fig. 4 it is clear that inside the GO membrane water molecules have more interaction with the hydrophobic carbon wall for

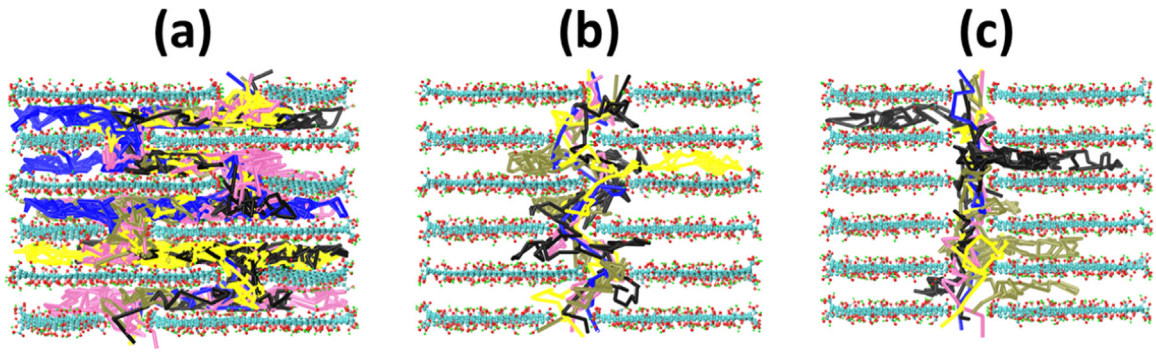

Fig. 4. Trajectory of water molecules through the 3 GO membrane configurations; (a) configuration-1, (b) configuration-2, (c) configuration-3. Trajectory path for 5 different water molecules are considered and their trajectory paths are shown with different colors. In the membrane red color is for oxygen atoms, green color is for hydrogen atoms and cyan color is for carbon atoms (For interpretation of the references to color in this figure legend, the reader is referred to the web version of this article.).

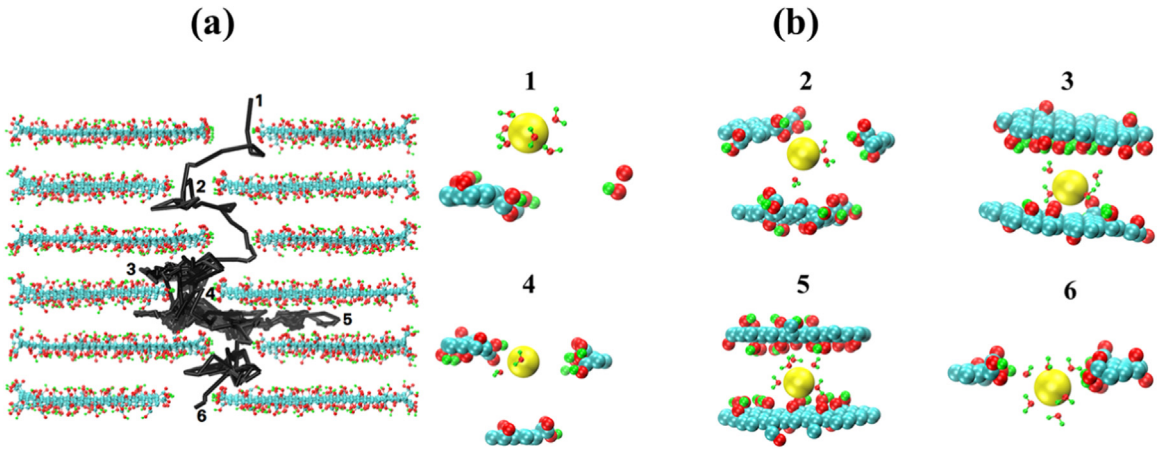

Fig. 5. (a) Trajectory of Na^+ ion inside the layered GO membrane for configuration-2. (b) Number of water molecules in the hydration shell of the Na^+ ion while crossing the membrane. Cyan color is for carbon atoms, red color is for oxygen atoms, green color is for hydrogen atoms and yellow color is for Na^+ ion (For interpretation of the references to color in this figure legend, the reader is referred to the web version of this article.).

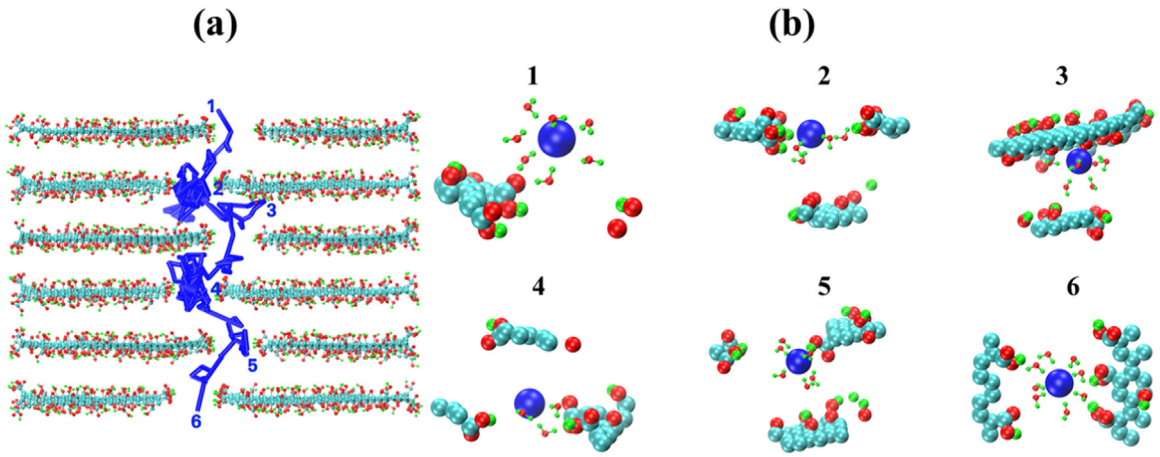

Fig. 6. (a) Trajectory of Cl^- ion inside the layered GO membrane for configuration-2. (b) Number of water molecules in the hydration shell of the Cl^- ion while crossing the membrane. Cyan color is for carbon atoms, red color is for oxygen atoms, green color is for hydrogen atoms and blue color is for Cl^- ion (For interpretation of the references to color in this figure legend, the reader is referred to the web version of this article.).

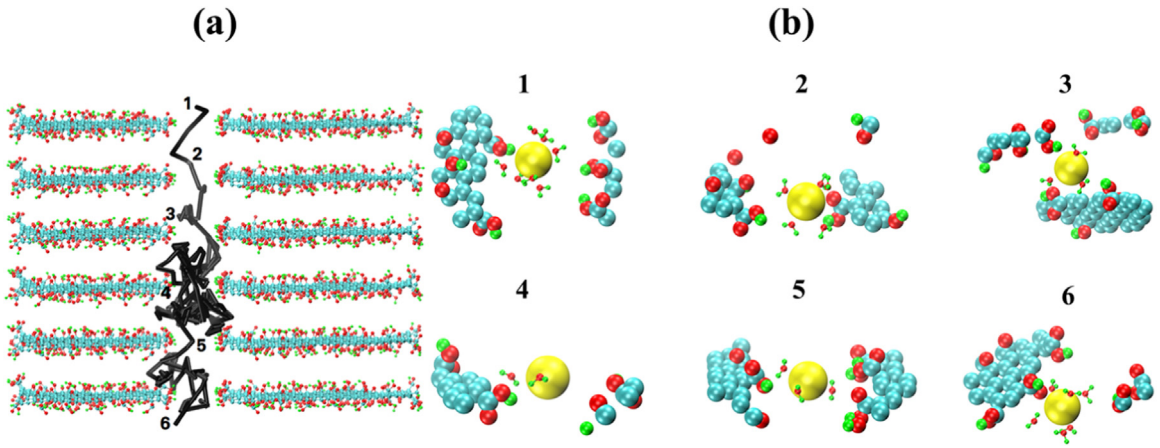

Fig. 7. (a) Trajectory of Na^+ ion inside the layered GO membrane for configuration-3. (b) Number of water molecules in the hydration shell of the Na^+ ion while crossing the membrane. Cyan color is for carbon atoms, red color is for oxygen atoms, green color is for hydrogen atoms and yellow color is for Na^+ ion (For interpretation of the references to color in this figure legend, the reader is referred to the web version of this article.).

configuration-1 (Fig. 4a) followed by configuration-2 (Fig. 4b) and configuration-3 (Fig. 4c). It is remarkable to observe that the velocity of water molecules inside the GO channels is maximum for configuration-3 followed by configuration-2 and configuration-1, as depicted in Figs. 10g, 10h, 10i, which is in contrary to the previous observations that the high water permeability through the GO membrane is due to the frictionless flow of water through atomically smooth hydrophobic carbon wall [29,31]. It is the pore offset distance (**W**) of the GO

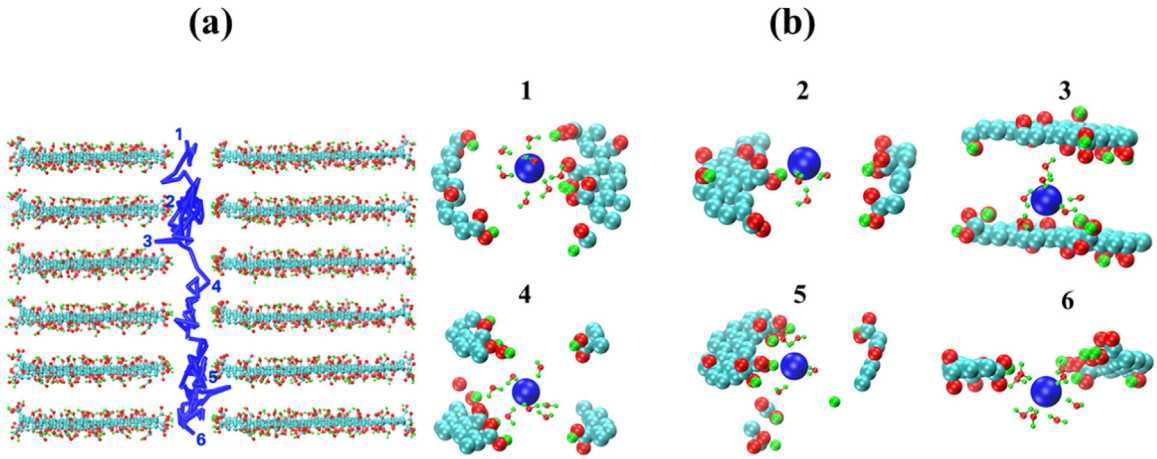

Fig. 8. (a) Trajectory of Cl- ion inside the layered GO membrane for configuration-3. (b) Number of water molecules in the hydration shell of the Cl^- ion while crossing the membrane. Cyan color is for carbon atoms, red color is for oxygen atoms, green color is for hydrogen atoms and blue color is for Cl^- ion (For interpretation of the references to color in this figure legend, the reader is referred to the web version of this article.).

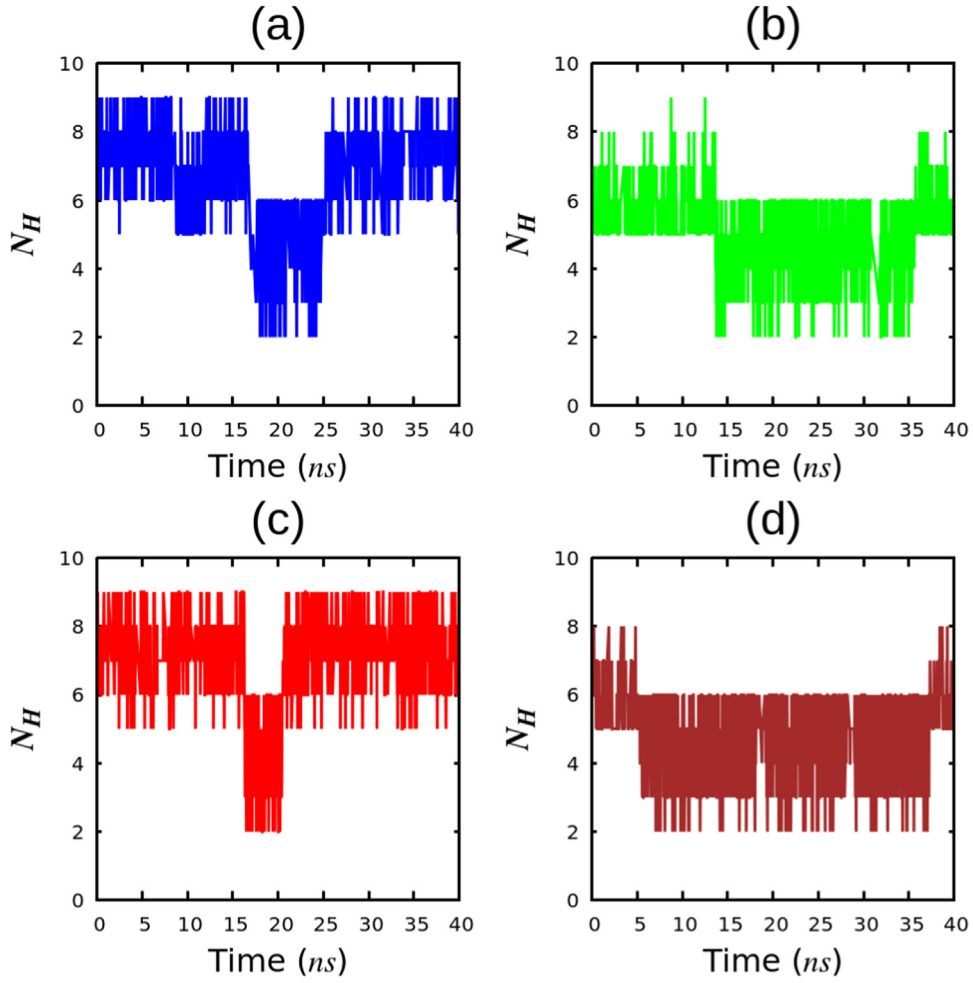

Fig. 9. Variation of number of water molecules in the hydration shell of the ions as a function of the simulation time. (a) Cl^- ion for configuration-2 (b) Na^+ ion for configuration-2 (c) Cl^- ion for configuration-3 (d) Na^+ ion for configuration-3.

membrane or the size of the constituting GO sheets of the membrane that has a major role to play on the water permeation and salt rejection.

3.1. Experimental observation

In order to verify simulation results, GO samples of three different average sheet sizes were separated from GO dispersion prepared by employing modified Hummers method. As synthesized GO samples are highly polydisperse in their lateral dimensions, typically in the range of 0.5–20.0 μm. Sheets were sorted into different groups of uniform sizes via simple centrifugation process [35]. Large GO sheets were selectively settled down by centrifuging the aqueous dispersion of pristine GO

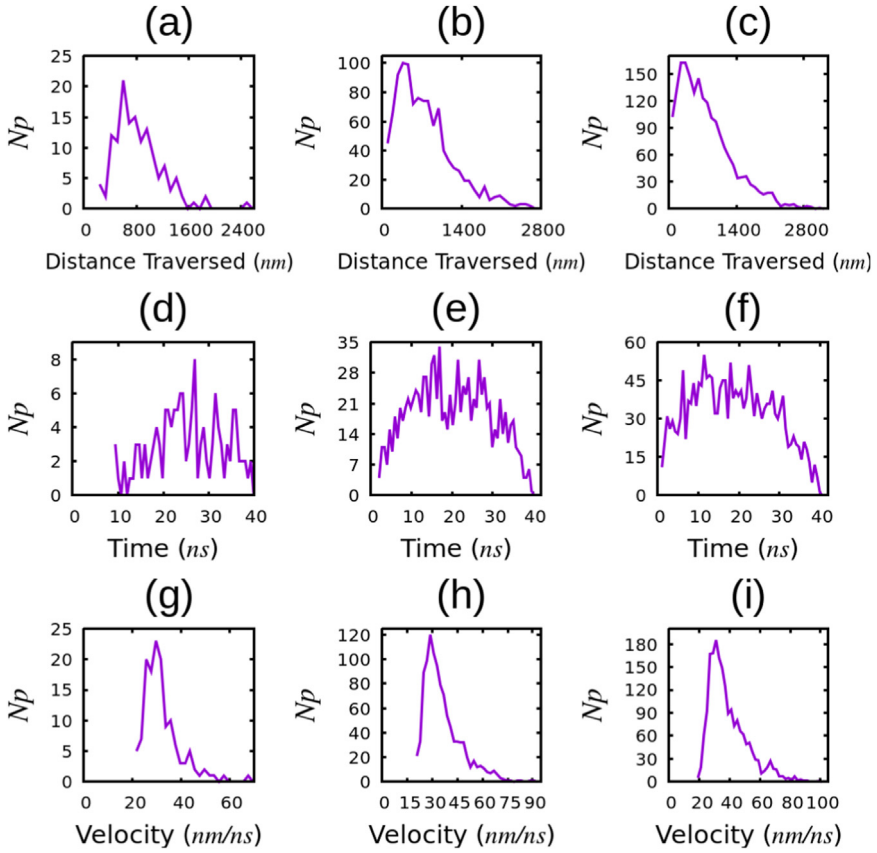

Fig. 10. Distribution of distance traversed, time taken by the water molecules and their velocity while permeating through the GO membranes, for three different configurations (Configuration 1: 1st column, Configuration 2: 2nd column and Configuration 3: 3rd column).

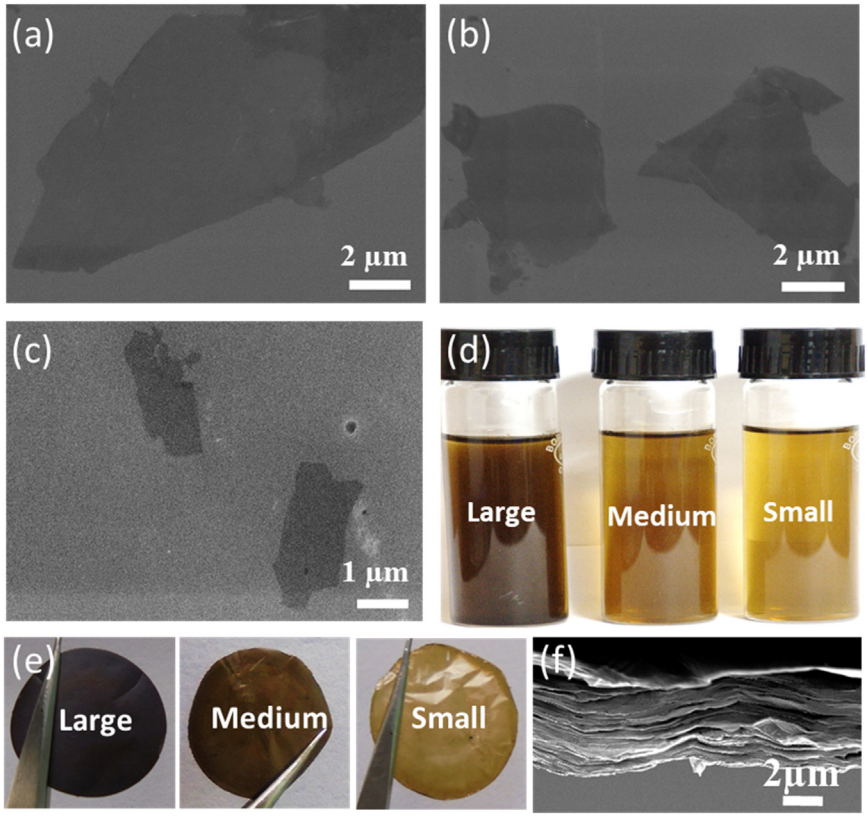

Fig. 11. FESEM image of (a) large, (b) medium, and (c) small GO sheet. (d) Aqueous dispersions of large, medium and small GO sheet (e) Digital photograph of the free-standing membranes prepared from large, medium and small GO Sheet (f) Cross-sectional FESEM image of a GO membrane (For interpretation of the references to color in this figure, the reader is referred to the web version of this article.).

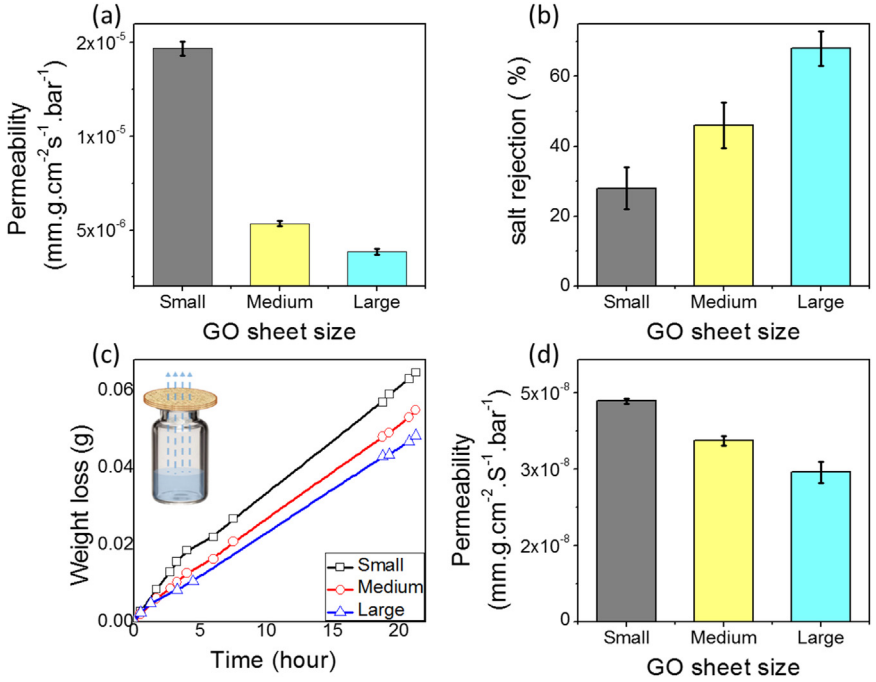

Fig. 12. (a) Rate of water permeation, (b) Salt rejection performance, and (c) Rate of evaporation of water through different GO membranes (d) Rate of water vapor permeation through GO membrane prepared from dispersions of sheets of different lateral dimensions.

sample at 2000 rotation per minute (rpm) and named as “large GO”. A representative FESEM image of large GO is shown in Fig. 11a. GO sheets with smaller lateral dimensions were remained dispersed in the supernatant solution even after centrifugation at 2000 rpm, this fraction of sheets is named as “medium GO”. A sample of medium GO was further sonicated for 2 h, in a bath sonicator to cleave the sheets into smaller fragments, and named as “small GO”. Representative FESEM images of medium and small GO sheets are shown in Figs. 11b and 11c, respectively. With changing lateral dimensions of the GO sheets, the appearance of dispersions was changed. As can be seen in Fig. 11d, dispersion of large GO sheets appeared to be dark brown, while that of small GO looks light yellow in color. In order to prepare freestanding membranes of GO sheets of different sizes, aqueous dispersions of each GO samples (2 mg) were vacuum filtered through cellulose nitrate membranes with a pore dimension of 100 nm. Digital photo of GO membranes prepared as such are shown in Fig. 11e, similar to the dispersions, the color of the membrane prepared with larger GO sheets appeared to be dark brown and that of small GO is seen as light brown. The cross-sectional FESEM image in Fig. 11f clearly reveals the lamellar structure of reconstructed GO membranes. In order to estimate the rate of liquid water permeation through as prepared membranes, the time required to vacuum filter 2 ml of DI water through different GO membranes were noted. The permeability constants were calculated by employing Eq. (8).

$$Permeability = \frac{(membrane\ thickness) \times (amount\ of\ permeate)}{(membrane\ surface\ area) \times (time) \times (differential\ pressure)} \quad (8)$$

In Fig. 12a, the rate of liquid water permeation through the membranes of different GO sizes are shown. Data of four representative repetition of permeability experiment is shown in the Supporting table 1. Similar to configuration-1 of Fig. 2a, in the membranes of large GO sheets water molecules had to travel through a zig-zag route of longer distance, and hence it displayed the lowest permeability. On the other hand, membranes of small GO sheets resembling configuration-3 of Fig. 2c provided shorter and straight pathways for the water molecules to permeate and hence displayed the highest permeability. In an analogues experiment, the salt rejection performance of different GO membranes was studied by vacuum filtering 100 ppm aqueous solution of NaCl. The concentration of Na^+ in the filtrate was determined by employing a flame photometer instrument (Analab, μFlameCal10). Fig. 12b, shows bar diagrams of salt rejection performance of membranes prepared from GO sheet of different sizes. Here again, salt rejection performance is found to be proportional to the lengths of the nanochannels. The membrane of “large GO” with zig-zag nanochannels (configuration-1) displayed highest rejection performance and membrane of “small GO” with straight and short pathways (configuration-3) shown the lowest rejection rate.

In order to get further insights into the effect of nanochannels geometry on water permeation rate, permeation of water vapors through GO membranes of different sheets sizes was studied gravimetrically [13,45]. In this study, glass ampoules (5 ml capacity) containing 3 ml of water were sealed with the membranes using a freshly prepared polydimethylsiloxane (PDMS) elastomer. A schematic of the set-up is shown in Fig. 12c as an inset. The sealed ampoules were stored in a chamber with the relative humidity controlled at 22%. The rate of water evaporation through the membranes was determined by measuring weight of the ampules at consistent time intervals. The rate of the weight loss of sealed ampules is dictated by the permeability of sealing membranes. As can be seen from Fig. 12c, ampules sealed with “small GO” membranes shown weight loss at a faster rate than that of “large GO” membranes. The weight loss data of three representative repetition of vapor permeability experiment is shown in the supporting Fig. 1. From the weight loss data, the vapor permeability of the membranes were calculated by using Eq. (8) and shown in Fig. 12d. Here again, the membrane of “large GO” (configuration-1) displayed lower permeability than that of “small GO” (configuration-3). The membrane of “large GO” represents a system with unfavorable geometry having long zigzag nanochannels, but it contains regions of hydrophobic surface favorable for water flow (the regions of aromatic carbons in the basal plan of GO exhibiting frictionless flow of water). On the other hand membrane of “small GO” represents a system of favorable geometry having relatively shorter and straight nanochannels but the path is unfavorable for water flow due to the hydrophilic edges of GO sheets. Our experimental and simulated results suggest that in this competition of favorable geometry vs favorable surface, channels with favorable

geometry show better water permeability.

4. Conclusions

Combined experimental and molecular dynamics simulation study conclude that the interaction between the hydrophobic carbon wall of the GO membrane and water molecules does not seem to affect the water permeation through the membrane. It is the pore offset distance (**W**) of the GO membrane that has a major role to play on the water permeation and salt rejection through the membrane. As the size of the GO sheets, which constitute the membrane, decreases, the water molecules have to traverse a "less zig-zag" path to permeate through the membrane. So they have to cover a lesser distance during permeation and trapped inside the membrane configuration for a smaller duration of time. As a consequence, the water permeability of the membrane increases, but the salt rejection decreases at the same time. So, the water permeation and salt rejection of the GO membrane can aptly be tuned with proper selections of the pore offset distance (**W**) or selecting the appropriate size of the constituting GO sheets.

Acknowledgements

A. Gogoi and K. Anki Reddy would like to thank Param-Ishan High Performance Computing facility, IIT Guwahati. K. Raidongia acknowledge Ramanujan Research Grant (SB/S2/RJN-141/2014) of Science and Engineering Research Board (SERB), India for financial support. K. Raidongia and T. J. Konch would like to thank Central Instrumental Facility (CIF), IIT Guwahati for the help with sample characterization.

Appendix A. Supporting information

Supplementary data associated with this article can be found in the online version at http://dx.doi.org/10.1016/j.memsci.2018.06.031.

References

[1] Z.B. Ye, Y. Xu, H. Chen, C. Cheng, L.J. Han, L. Xiao, A novel micro nano structure profile control agent: graphene oxide dispersion, J. Nanomater. 2014 (582089) (2014) 1–9.
[2] J. Chen, Y. Li, L. Huang, N. Jia, C. Li, G. Shi, Size fractionation of graphene oxide sheets via filtration through track-etched membranes, Adv. Mater. 27 (2015) 3654–3660.
[3] R.K. Joshi, P. Carbone, F.C. Wang, V.G. Kravets, Y. Su, I.V. Grigorieva, H.A. Wu, A.K. Geim, R.R. Nair, Precise and ultrafast molecular sieving through graphene oxide membranes, Science 343 (2014) 752–754.
[4] A. Kim, L.J. Cote, J. Huang, Two dimensional soft material: new faces of graphene oxide, Acc. Chem. Res. 45 (8) (2012) 1356–1364.
[5] R. Devanathan, D.C. Woods, Y. Shin, D.W. Gotthold, Molecular dynamics simulations reveal that water diffusion between graphene oxide layers is slow, Sci. Rep. 6 (29484) (2016) 1–8.
[6] H. Dai, Z. Xu, X. Yang, Water permeation and ion rejection in layer-by- layer stacked graphene oxide nanochannels: a molecular dynamics simulation, J. Phys. Chem. C 120 (2016) 22585–22596.
[7] N. Wei, X. Peng, Z. Xu, Understanding water permeation in graphene oxide membranes, Appl. Mater. Interfaces 6 (2014) 5877–5883.
[8] N. Raghav, S. Chakraborty, P.K. Maiti, Molecular mechanism of water permeation in a helium impermeable graphene and graphene oxide membrane, Phys. Chem. Chem. Phys. 17 (2015) 20557–20562.
[9] J.A.L. Willcox, H.J. Kim, Molecular dynamics study of water flow across multiple layers of pristine, oxidized, and mixed regions of graphene oxide, ACS Nano 11 (2017) 2187–2193.
[10] R.K. Joshi, S. Alwarappan, M. Yoshimura, V. Sahajwalla, Y. Nishina, Graphene oxide: the new membrane material, Appl. Mater. Today 1 (1) (2015) 1–12.
[11] J.R. Werber, C.O. Osuji, M. Elimelech, Materials for next-generation desalination and water purification membranes, Nat. Rev. 1 (16018) (2016) 1–16.
[12] K. Raidongia, J. Huang, Nanofluidic ion transport through reconstructed layered materials, J. Am. Chem. Soc. 134 (2012) 16528–16531.
[13] R.R. Nair, H.A. Wu, P.N. Jayaram, I.V. Grigorieva, A.K. Geim, Unimpeded permeation of water through helium-leak–tight graphene-based membranes, Science 335 (2012) 442–444.
[14] A. Buchsteiner, A. Lerf, J. Pieper, Water dynamics in graphite oxide investigated with neutron scattering, J. Phys. Chem. B 110 (2006) 22328–22338.
[15] A. Lerf, A. Buchsteiner, J. Pieper, S. Schöttl, I. Dekanny, T. Szabo, H.P. Boehm, Hydration behavior and dynamics of water molecules in graphite oxide, J. Phys. Chem. Solids 67 (2006) 1106–1110.
[16] S. Ban, J. Xie, Y. Wang, B. Jing, B. Liu, H. Zhou, Insight into the nanoscale mechanism of rapid H_2O transport within a graphene oxide membrane: impact of oxygen functional group clustering, Appl. Mater. Interfaces 8 (2015) 321–332.
[17] X.L. Xu, F.W. Lin, Y. Du, X. Zhang, J. Wu, Z.K. Xu, Graphene oxide nanofiltration membranes stabilized by cationic porphyrin for high salt rejection, Appl. Mater. Interfaces 8 (2016) 12588–12593.
[18] Y.H. Xi, J.Q. Hu, Z. Liu, R. Xie, X.J. Ju, W. Wang, L.Y. Chu, Graphene oxide membranes with strong stability in aqueous solutions and controllable lamellar spacing, Appl. Mater. Interfaces 8 (2016) 15557–15566.
[19] W. Wang, E. Eftekhari, G. Zhu, X. Zhang, Z. Yan, Q. Li, Graphene oxide membranes with tunable permeability due to embedded carbon dots, ChemComm 50 (2014) 13089–13092.
[20] F. Perreault, A.F. de Fariaa, M. Elimelech, Environmental applications of graphene-based nanomaterials, Chem. Soc. Rev. 44 (2015) 5861–5896.
[21] W.S. Hung, Q.F. An, M. De Guzman, H.Y. Lin, S.H. Huang, W.R. Liu, C.C. Hu, K.R. Lee, J.Y. Lai, Pressure-assisted self-assembly technique for fabricating composite membranes consisting of highly ordered selective laminate layers of amphiphilic graphene oxide, Carbon 68 (2014) 670–677.
[22] L.S. Fifield, Y. Shin, W. Liu, D.W. Gotthold, Scalable production method for graphene oxide water vapor separation membranes, Mater. Res. Soc. Adv. 1 (28) (2016) 2091–2098.
[23] M. Lamb, G.W. Koch, E.R. Morgan, M.W. Shafer, A synthetic leaf: the biomimetic potential of graphene oxide, Proc. SPIE - Int. Soc. Opt. Eng. 9429 (2015) 1–10.
[24] L.G. Cruz, C.C. Coterillo, Á. Irabien, V. Montiel, J. Iniesta, High performance of alkaline anion-exchange membranes based on chitosan/poly (vinyl) alcohol doped with graphene oxide for the electrooxidation of primary alcohols, J. Carbon Res. 2 (10) (2016) 1–19.
[25] S.H.M. Akhair, Z. Harunb, M.R. Jamalludinb, M.F. Shuhord, N.H. Kamarudina, M.Z. Yunosb, A. Ahmada, M.F.H. Azhar, Polymer mixed matrix membrane with graphene oxide for humic acid performances, Chem. Eng. Trans. 56 (2017) 697–702.
[26] Y. Shin, W. Liu, B. Schwenzer, S. Manandhar, D.C. Woods, M.H. Engelhard, R. Devanathan, L.S. Fifield, W.D. Bennett, B. Ginovska, Graphene oxide membranes with high permeability and selectivity for dehumidification of air, Carbon 106 (2016) 164–170.
[27] Y. You, V. Sahajwalla, M. Yoshimura, R.K. Joshi, Graphene and graphene oxide for desalination, Nanoscale 8 (2016) 117–119.
[28] C.N. Yeh, K. Raidongia, J. Shao, Q.-H. Yang, J. Huang, On the origin of the stability of graphene oxide membranes in water, Nat. Chem. 7 (2015) 166–170.
[29] K. Huang, G. Liu, Y. Lou, Z. Dong, J. Shen, W. Jin, A graphene oxide membrane with highly selective molecular separation of aqueous organic solution, Angew. Chem. Int. Ed. 53 (2014) 6929–6932.
[30] D. An, L. Yang, T.J. Wang, B. Liu, Separation performance of graphene oxide membrane in aqueous solution, Ind. Eng. Chem. Res. 55 (2016) 4803–4810.
[31] H. Huang, Z. Song, N. Wei, L. Shi, Y. Mao, Y. Ying, L. Sun, Z. Xu, X. Peng, Ultrafast viscous water flow through nanostrand-channelled graphene oxide membranes, Nat. Commun. 4 (2979) (2013) 1–9.
[32] L.C. Lin, J.C. Grossman, Atomistic understandings of reduced graphene oxide as an ultrathin-film nanoporous membrane for separations, Nat. Commun. 6 (8335) (2015) 1–7.
[33] W.L. Tong, W.J. Ong, S.P. Chai, M.K. Tan, Y.M. Hung, Enhanced evaporation strength through fast water permeation in graphene-oxide deposition, Sci. Rep. 5 (11896) (2015) 1–13.
[34] Y. Han, Y. Jiang, C. Gao, High-flux graphene oxide nanofiltration membrane intercalated by carbon nanotubes, Appl. Mater. Interfaces 7 (2015) 8147–8155.
[35] X. Lin, X. Shen, Q. Zheng, N. Yousefi, L. Ye, Y.W. Mai, J.K. Kim, Fabrication of highly-aligned, conductive, and strong graphene papers using ultralarge graphene oxide sheets, ACS Nano 6 (2012) 10708–10719.
[36] A. Lerf, H. He, M. Forster, J. Klinowski, Structure of graphite oxide revisited, J. Phys. Chem. B 102 (1998) 4477–4482.
[37] H. Tang, D. Liu, Y. Zhao, X. Yang, J. Lu, F. Cui, Molecular dynamics study of the aggregation process of graphene oxide in water, J. Phys. Chem. C 119 (2015) 26712–26718.
[38] C.J. Shih, S. Lin, R. Sharma, M.S. Strano, D. Blankschtein, Understanding the pH-dependent behavior of graphene oxide aqueous solutions: a comparative experimental and molecular dynamics simulation study, Langmuir 28 (2012) 235–241.
[39] W. Humphrey, A. Dalke, K. Schulten, VMD-visual molecular dynamics, J. Mol. Graph. 14 (1996) 33–38.
[40] J.C. Phillips, R. Braun, W. Wang, J. Gumbart, E. Tajkhorshid, E. Villa, C. Chipot, R.D. Skeel, L. Kalé, K. Schulten, Scalable molecular dynamics with NAMD, J. Comput. Chem. 26 (2005) 1781–1802.
[41] W.L. Jorgensen, D.S. Maxwell, J.T. Rives, Development and testing of the OPLS all-atom force field on conformational energetics and properties of organic liquids, J. Am. Chem. Soc. 118 (45) (1996) 11225–11236.
[42] W.L. Jorgensen, J. Chandrasekhar, J.D. Madura, Comparison of simple potential functions for simulating liquid water, J. Chem. Phys. 79 (1983) 926–935.
[43] S. Miyamoto, P.A. Kollman, Settle: an analytical version of the SHAKE and RATTLE algorithm for rigid water models, J. Comput. Chem. 13 (1992) 952–962.
[44] U. Essmann, L. Perera, M.L. Berkowitz, A smooth particle mesh Ewald method, J. Chem. Phys. 103 (1995) 8577–8593.
[45] R.K. Gogoi, K. Saha, J. Deka, D. Brahma, K. Raidongia, Solvent-driven responsive bilayer membranes of clay and graphene oxide, J. Mater. Chem. A 5 (2017) 3523–3533.